Supporting Information

Direct Writing Electrospinning of Scaffolds with Multi-dimensional Fiber Architecture for Hierarchical Tissue Engineering

Honglin Chen[§], Afonso de Botelho Ferreira Braga Malheiro[§], Clemens van Blitterswijk, Carlos Mota, Paul Andrew Wieringa, Lorenzo Moroni*

H. Chen, A. Malheiro, Prof. C. A. Van Blitterswijk, Dr. C. Mota, Dr. P. Wieringa and Prof. L. Moroni

Department of Complex Tissue Regeneration

MERLN Institute for Technology-Inspired Regenerative Medicine

Maastricht University

6200 MD Maastricht, The Netherlands

*Corresponding author: l.moroni@maastrichtuniversity.nl.

[§] These authors contributed equally to this manuscript.

1. Materials and Methods

Polymer Solution Characterization

Viscosity

Viscosity measurements were performed at 25^0C using a rheometer (MCR702 TwinDrive, Anton Paar) with a two parallel plate configuration and operating in rotational mode. The viscosity of solutions of 28% 300PEOT55PBT45 in 75/25 $CHCl_3$/HFIP and 20% PCL in 75/25 $CHCl_3$/HFIP was registered while varying the shear stress (1/s) from 0 to 100. Three measurements were done per sample and the best fitting curve derived from these.

Surface Tension

The evaluation of the polymers solution's surface tension was carried out using an optical contact angle measuring system (OCA 20, Dataphysics) at 25 °C. Since the organic solvents in the solution have high evaporation rates, the preferred method for surface tension measuring was an axisymmetric drop shape analysis (ADSA) of an air bubble/polymer solution interface. ADSA is a powerful tool for fast, accurate and reliable measurements of fluid-liquid interfacial tensions. ADSA is based on the numerical fit between the shape of an experimental bubble (or drop) and the mathematical model given by the classical Laplace equation of capillarity[1]. In this procedure, a closed container was filled with the polymer solution and a capillary (with the tip bent upwards) was dipped in it. An air bubble was precisely dosed through the capillary and the evolution of the drop shape and contact angle was automatically analysed and used to extrapolate the surface tension. The surface tension of deionized (DI) water at 25 °C (γ=71.99 ± 0.005) was used as an accuracy control.

Conductivity

Conductivity measurements were obtained using an impedance spectroscopy-based method. Impedance spectroscopy provides the relation between the real (Zr) and imaginary (Zi) impedance of a sample, as a function of the applied frequency, and the results can then be graphically expressed in the Nyquist plot, as Zr v. Zi. The impedance of a resistance is independent of the frequency, and thus it has no imaginary part [25]. Hence, it is possible to determine the resistance of a solution from a Nyquist plot by fitting

the resulted curve and calculating the impedance when the imaginary part is zero. Once determining the resistance (R), the electrical resistivity of a solution (ρ) can be determined using the relation R = ρ (L/A), where L is the distance between the electrodes and A is the area of the electrode. To determine these parameters precisely, solutions of known conductivity (σ) can be used to calibrate the system, since σ=1/ρ. Potassium chloride (KCl) solutions of 1M, 0.1M, 0.01M, 0.001M and 0.0001M were then prepared and the resistance measured. The results were fitted into a curve and the calibration factor of the system (L/A) could then be determined. Finally, to obtain the polymer solution conductivity, the resistance was first measured through the Nyquist plot fit and the conductivity calculated using the calibration factor. The impedance spectroscopy measurements were carried using the Autolab software (Metrohm Autolab B.V.) and using a setup built in-house.

2. Figures

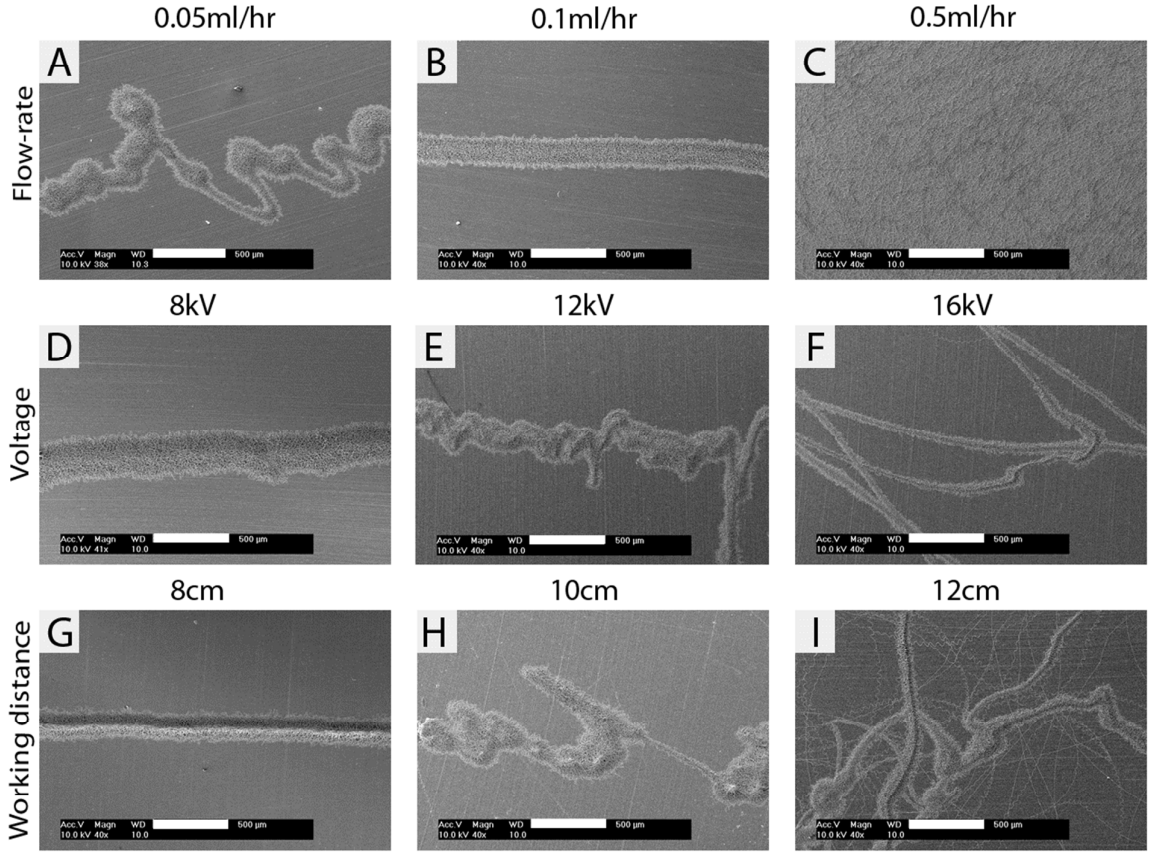

Figure S1. Influence of the processing parameters on the deposited line consistency. This gross examination was used to identify the direct writing region. (A–C) Effect of different flow rates at a voltage (V) is 8 kV and working distance (Wd) of 8 cm; (D–F) Effect of the voltages at Wd=8 cm and flow-rate is

0.08 mL/h; (G–I) Effect of different working distance at V=8 kV and the flow-rate is 0.08mL/h Scale bars: A–I (500 μm).

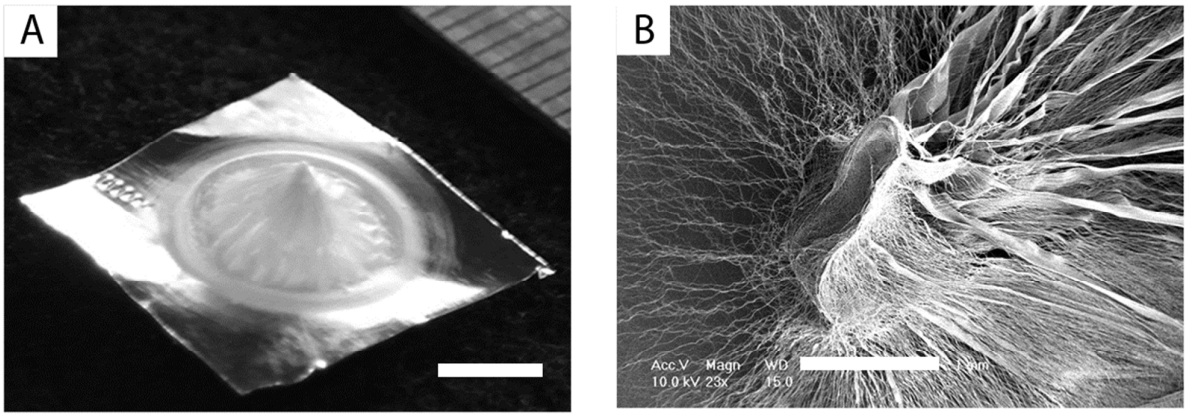

Figure S2. Point pattern created when the solution is let to spin at a single point for a prolonged period. (A) Digital camera image; (B) SEM micrograph. Scale bars: A (5 mm) and B (1 mm).

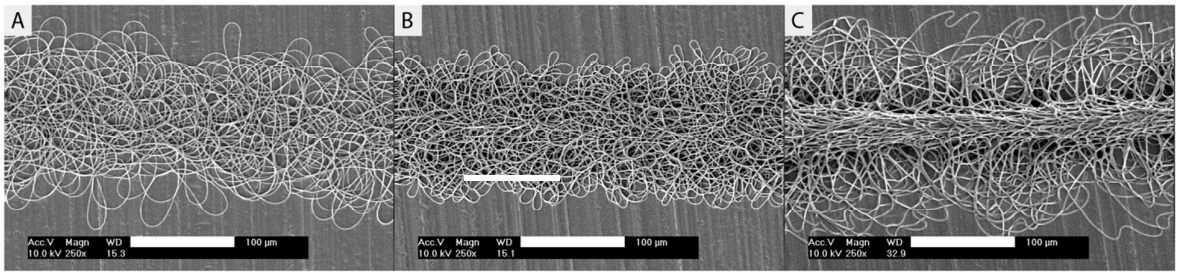

Figure S3. Bundle morphology resulting from different voltages: (A) 4 kV, (B) 5 kV and (C) 6 kV. The working distance was maintained at 5 cm, the flow-rate at 0.18 mL/h and the scan-speed at 10 mm/s. Scale bars: A–C (100 μm).

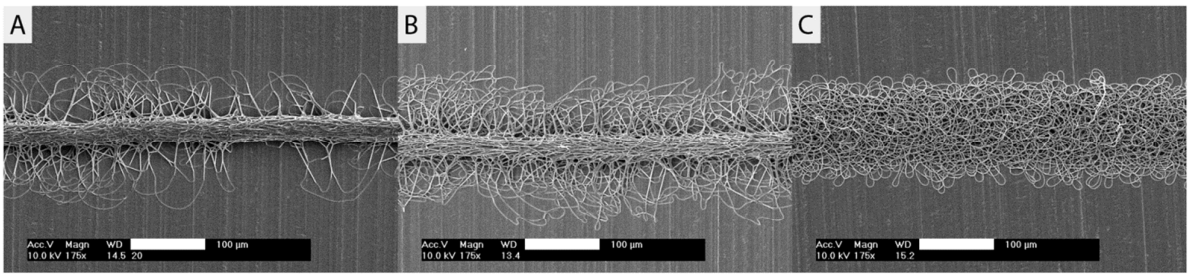

Figure S4. SEM images showing the effect of working distance on the deposited fibers at (A) Wd = 3 cm, (B) Wd = 4 cm and (C) Wd = 5 cm. The applied voltage was set at 5kV, the flow-rate at 0.18 mL/h and the scan speed at 10 mm/s. Scale bars: A–C (100 μm).

.

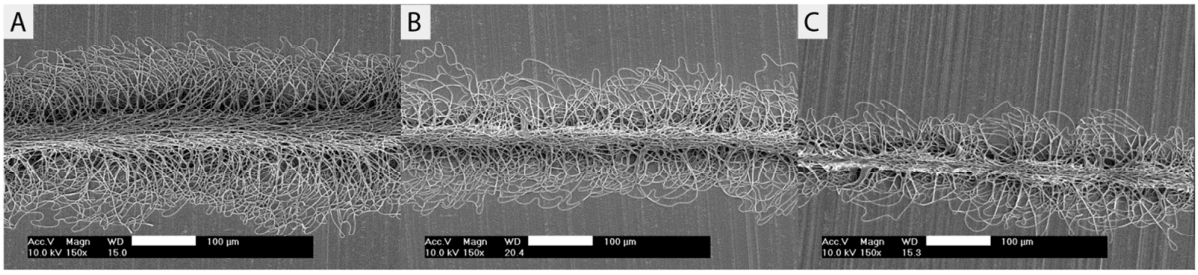

Figure S5. Effect on the line pattern at different scan speeds (A) 4 mm/s, (B) 7 mm/s and (C) 10 mm/s. The voltage was set at 5 kV, the working distance at 5 cm and the flow-rate at 0.18 mL/h. Scale bars: A–C (100 *µ*m).

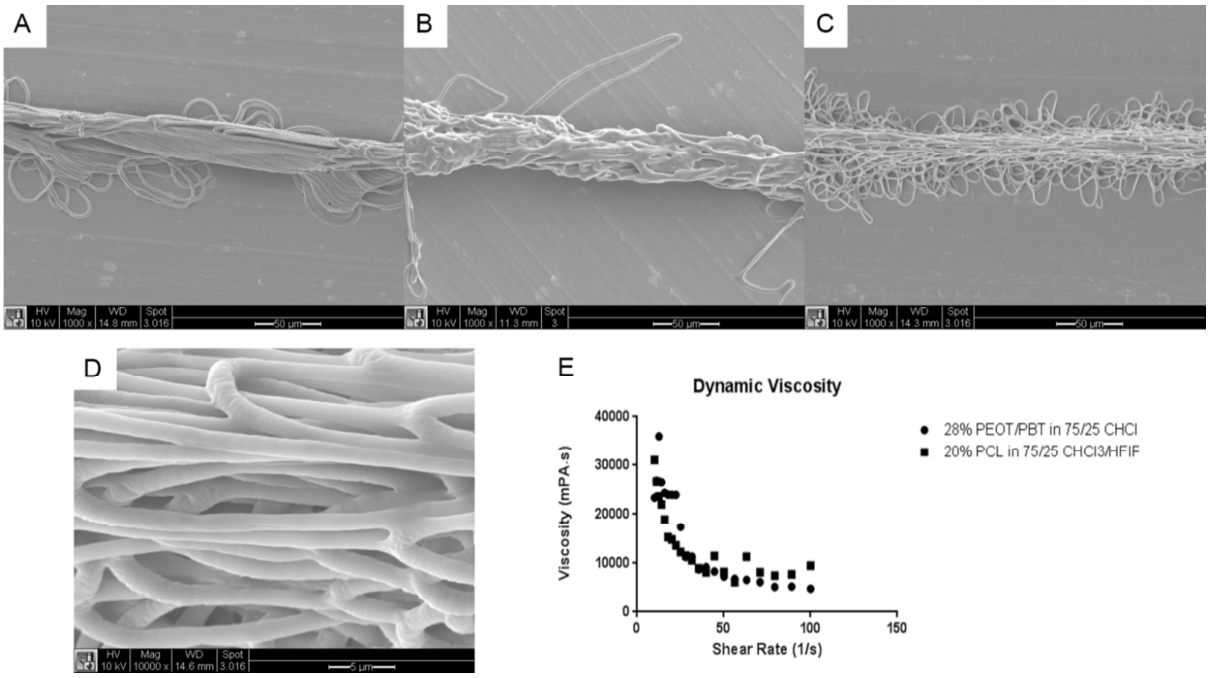

Figure S6. DW ESP with a solution of 20% PCL in 75/25 Chloroform/HFIP. (A-C) Effect of voltage on the fiber bundle, when the voltage is (A) 7 kV, (B) 8.5 kV and (C) 10 kV. The working distance is fixed at 4.5 cm, the flow-rate at 1ml/hr and the scan-speed at 10 mm/s. (D) High magnification of a fiber bundle represented in (C). The individual fiber diameter is 1.42 ± 0.09 *µ*m. (E) Comparison of viscosity between this PCL solution and the adopted PEOT/PBT solution. Scale bars: (A-C): 50 *µ*m; (D) 5 *µ*m.

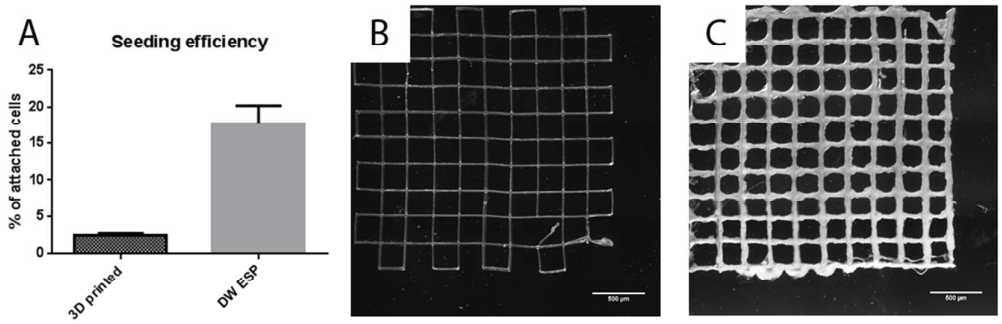

Figure S7. (A) Seeding efficiency of human mesenchymal stromal cells (hMSCs) on (B) 3D printed scaffolds and (C) direct-written (DW) electrospun (ESP) scaffolds. Efficiency measured as attached cells relative to total cells seeded on scaffolds and expressed as mean ± SD. Scale bars: B–C (500 μm).

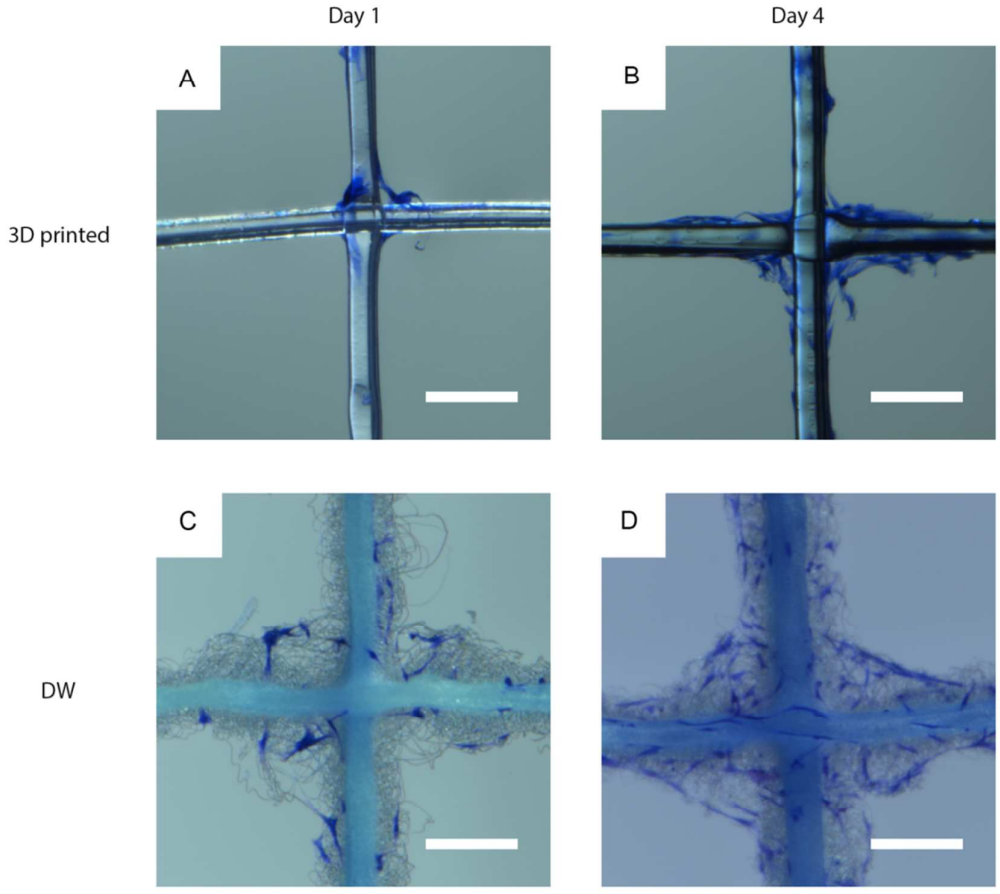

Figure S8. Methylene Blue staining on (A and B) 3D-printed and (C and D) DW ESP scaffolds after (A and C) 1 day and (B and D) 4 days of culture in basic medium. Both scaffolds have the same pore space of 860 μm and an average line width of 150 μm, although the DW scaffolds appear larger due to the fiber protrusions. Scale bars represent 500 μm.

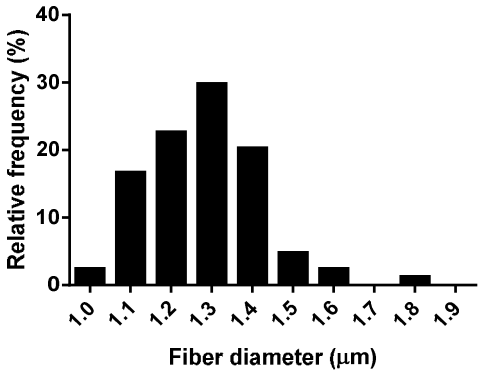

Figure S9. Frequency distribution of individual fiber diameters from the articular cartilage mimetic scaffold.

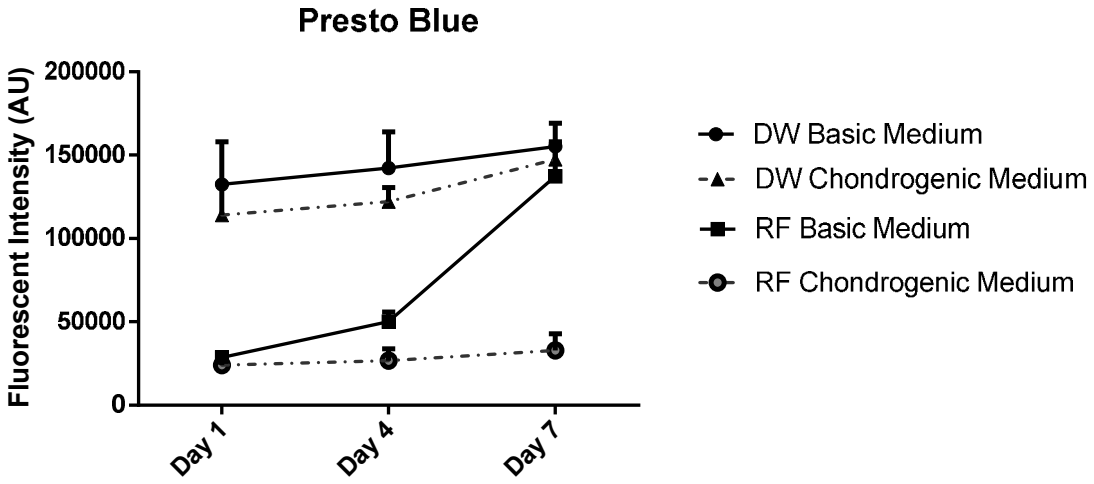

Figure S10. Presto blue measurements of the DW and RF seeded scaffolds taken at 3 times points during the first week of culture.

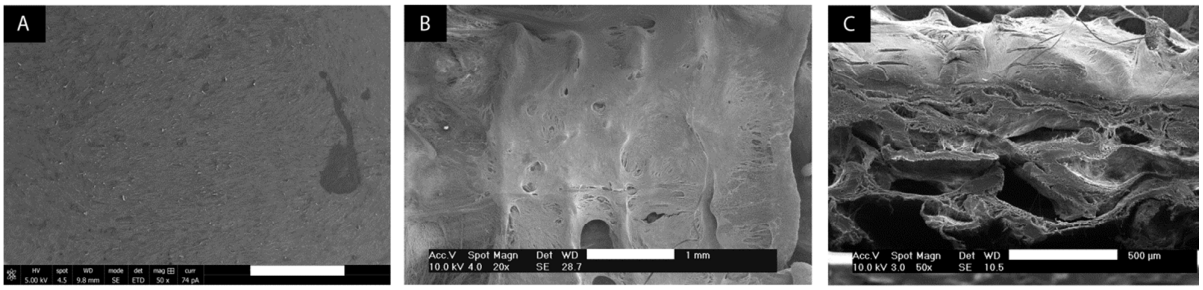

Figure S11. SEM micrographs of the cell-seeded scaffolds RF (A) and DW (B, C) after 21 days in culture on chondrogenic medium. (C) cross-section of the DW scaffold shows cells and matrix grow insides the scaffolds. Scale bars: A and B (1 mm), and C (500 μm).

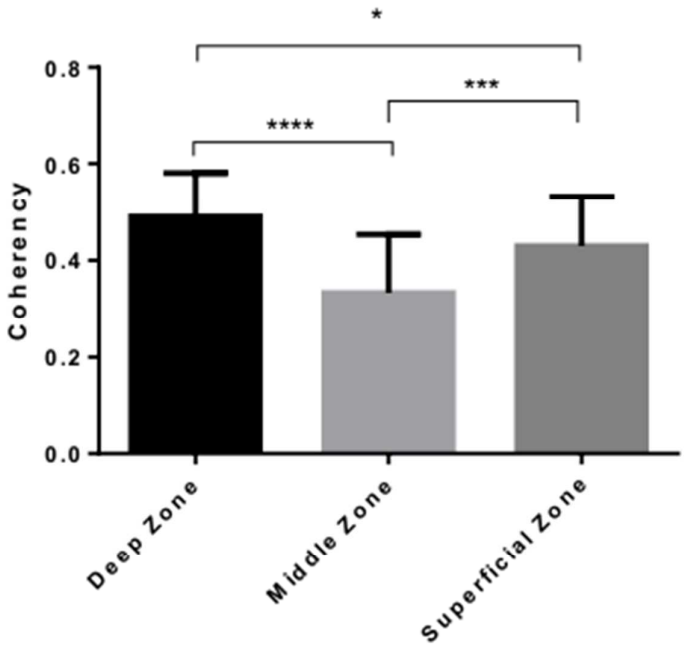

Figure S12. Directional coherency of the fibril matrix in the different sections of the DW ESP scaffold. 0 – no coherency; 1 – full coherency (full alignment). *p < 0.05; ***p < 0.001.

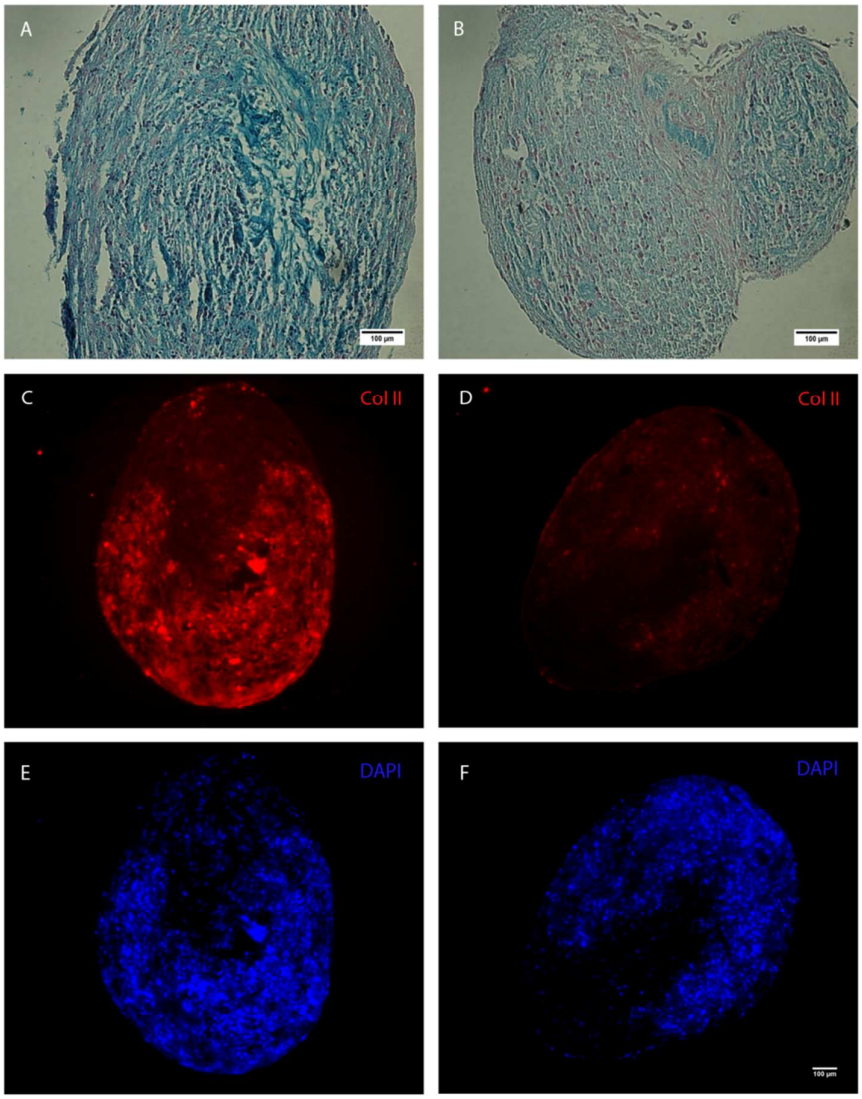

Figure S13. Chondrogenic differentiation of the hMSCs cultured in a pellet form in differentiation (left column) or control (right column) medium for 21 days. (A and B) Alcian Blue staining; (C and D) Collagen type II immunostaining; (E and F) DAPI staining. Scale bars: A–F (100 μm); scale bar in F applies to C–E panels.

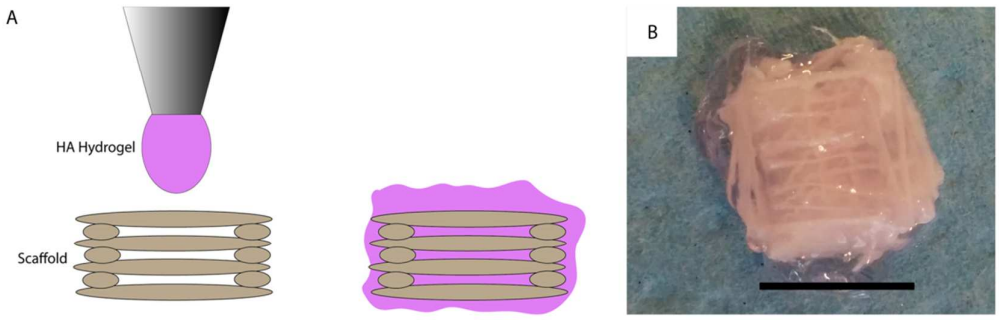

Figure S14. (A) Schematic of the process of scaffold embedding with a hyaluronic acid (HA) hydrogel and (B) photograph of such construct. Scale bars: 1 cm.

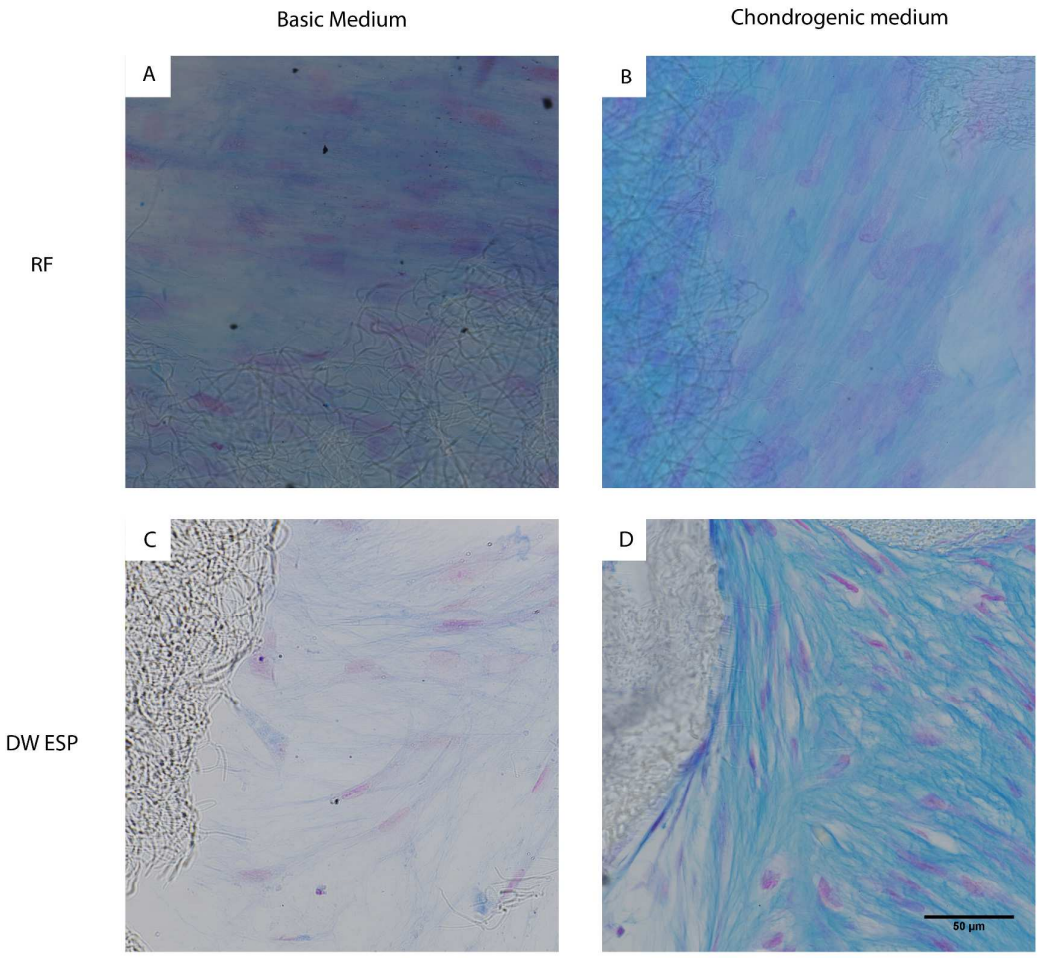

Figure S15. Alcian Blue and Nuclear Fast Red staining of histological sections of RF (A and B) and DW ESP (C and D) scaffolds after 21 days culture in basic (A and C) and chondrogenic medium (B and D). Scale bar in D represents 50 μm and applies to all panels.

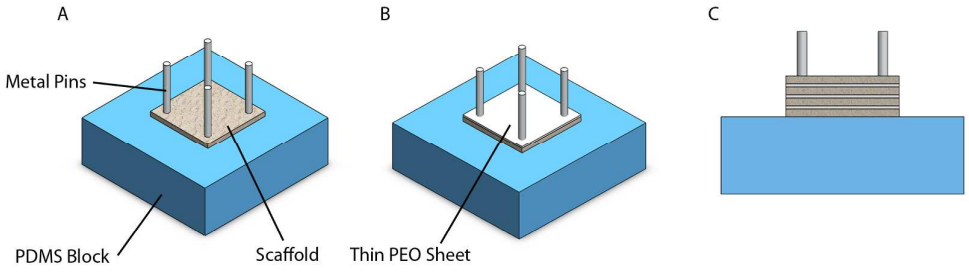

Figure S16. Scaffold mounting process: (A) The scaffold is placed on top of a PDMS block and fixed with thin metal bars; (B) a thin PEO sheet is then placed directly on top of the scaffold; (C) the process is repeated until 4 mats are assembled. The scaffold vertexes are then joined together and the sacrificial layers are dissolved in DI water.

3. Tables

Table S1. Review and comparison of current direct writing (DW) electrospinning (ESP) techniques

Manufacturing techniques	Advantages	Disadvantages	References
Solution ESP	• Moderate control over 3D pattern and scaffold size. • Works with a wide range of polymers. • Easy to produce fibers with diameter down to nanoscale level.	• Requires complex setups. • Difficult to produce single fibers at a time. • Unable to produce different fiber morphologies.	[2-5]
Near-field ESP	• Easy to obtain a fiber diameter in the nanoscale. • Well control over fiber pattern and shape. • Use of low voltages. • Easy to produce a single fiber at time.	• Difficulty in solvent evaporation due to low working distances. • Limited control over scaffold size (hard to scale-up). • Unable to produce different fiber morphologies.	[6-8]
Melt ESP	• Great shape fidelity. • Good resolution. • Easy to produce single fibers at a time. • Easy to scale-up due to a good fiber stacking. • No use of toxic solvents.	• The use of high temperature may cause polymer degradation. • Limited materials sources (thermoplastics only). • Difficulty in producing fibers down to the nanoscale. • Hard to add bioactive molecules. • Unable to produce different fiber morphologies.	[9-12]

Table S2. Summary of some physical properties from a solution of 28% PEO55PBT45 dissolved in 75:25 Chloroform:HFIP

Physical property	**Value**
Conductivity (μS/cm)	4.7 ± 0.2
Surface Tension (mN/m)	28.0 ± 0.7

Table S3. Summary of obtained fiber morphologies with varying working distances and voltages. The values in bold on the voltage column represent the minimum voltage for jet initiation. Once the jet starts to spin, the applied voltage can be reduced

Working Distance (cm)	Voltage (kV)	Focused spinning?	Morphology
2	2	N/A	N/A
	2.5	+	RF
	3	+	RF
	3.5	+	RF
	4	+	RF/AC
	4.5	+	SF
	5	-	–
3	3	N/A	N/A
	3.5	+	RF
	4	+	RF
	4.5	+	RF
	5	+	RF
	5.5	+	RF/AC
	6	+	AC
	7	–	–
4	3.5	N/A	N/A
	4	+	RF
	4.5	+	RF
	5	+	RF
	5.5	+	AC
	6	–	–

N/A, no spinning, no fiber RF, *Bundle of random fibers*
+, yes AC, *Bundle of fibers with aligned core*
– , *no* SF, *Single fiber*

Table S4. List of processing parameters that permitted DW ESP of PEOT/PBT

	Parameters	Range
	Polymer Solution	
▪	Concentration (w/v, %)	27–29
▪	$CHCl_3$:HFIP ratio (v/v)	74:26–78:22
	Process	
▪	Working distance (cm)	≤ 8
▪	Voltage (kV)	2.5 ≤ V ≤ 8
▪	Flow-rate (mL/h)	0.08 ≤ Q ≤ 0.3
▪	Scan-speed (mm/s)	≥5
	Ambient	
▪	Temperature (°C)	18.5–21
▪	Relative Humidity (%)	28–44

Table S5. Fiber alignment as a function of voltage and working distance

Voltage Effect

Voltage (V)	Working Distance (Wd)	V/Wd	Coherence value
4	5	0.80	0.135
5	5	1.00	0.190
6	5	1.20	0.377

Working Distance Effect

Voltage (V)	Working Distance (Wd)	V/Wd	Coherence value
5	3	1.67	0.505
5	4	1.25	0.474
5	5	1.00	0.178

Table S6. Characterization of the articular cartilage mimetic scaffold

Features	Value
Individual scaffold thickness (μm) Mounted scaffold thickness (mm)	208.5 ± 19.4 1.39 ± 0.6
Fiber diameter (μm)	1.39 ± 0.6
Pore Space Superficial zone (μm)	238.0 ± 79.3
Pore Space Deep zone (μm)	523.6 ± 156.2
Porosity (%)	91.2 ± 1.0
Young's Modulus in compression (MPa)	2.65 ± 0.65

Table S7. List of ESP parameters used for pattern and scaffold fabrication.

Parameter	Patterns/DW scaffold	RF sheet
Voltage (kV)	5	9
Working distance (cm)	3	4
Flow-rate (mL/h)	0.12	0.4
Scan-speed (mm/s)	35–50	5
Spinneret diameter (mm)	0.5	0.5
Temperature (°C)	18–21	20
Relative Humidity (%)	38–43	30–32

Table S8. List of qPCR primers sequence

Gene	Forward	Reverse
B2M	5'-ACAAAGTCACATGGTTCACA	5'-GACTTGTCTTTCAGCAAGGA
Col2a	5'-CGTCCAGATGACCTTCCTACG	5'-TGAGCAGGGCCTTCTTGAG
Sox9	5'-TGGGCAAGCTCTGGAGACTTC	5'-ATCCGGGTGGTCCTTCTTGTG
ACAN	5'-AGGCAGCGTGATCCTTACC	5'-GGCCTCTCCAGTCTCATTCTC
ALCAM	5'- ACGATGAGGCAGACGAGATAAGT	5'-CAGCAAGGAGGAGACCAACAAC

4. Video

Video S1: Solution electrospinning in a direct-writing approach.

Bibliography

1. Del Rıo, O.; Neumann, A., Axisymmetric Drop Shape Analysis: Computational Methods for the Measurement of Interfacial Properties from the Shape and Dimensions of Pendant and Sessile Drops. *J. Colloid Interface Sci.* **1997,** *196* (2), 136-147.
2. Lee, J.; Lee, S. Y.; Jang, J.; Jeong, Y. H.; Cho, D.-W., Fabrication of Patterned Nanofibrous Mats using Direct-write Electrospinning. *Langmuir* **2012,** *28* (18), 7267-7275.
3. Neubert, S.; Pliszka, D.; Góra, A.; Jaworek, A.; Wintermantel, E.; Ramakrishna, S., Focused Deposition of Electrospun Polymer Fibers. *J. Appl. Polym. Sci.* **2012,** *125* (1), 820-827.
4. Bellan, L. M.; Craighead, H., Control of an Electrospinning Jet Using Electric Focusing and Jet-Steering Fields. *J. Vac. Sci. Technol., B: Microelectron. Nanometer Struct.-Process., Meas., Phenom.* **2006,** *24* (6), 3179-3183.
5. Lee, J.; Jang, J.; Oh, H.; Jeong, Y. H.; Cho, D.-W., Fabrication of a Three-Dimensional Nanofibrous Scaffold with Lattice Pores Using Direct-Write Electrospinning. *Mater. Lett.* **2013,** *93*, 397-400.
6. Sun, D.; Chang, C.; Li, S.; Lin, L., Near-Field Electrospinning. *Nano Lett.* **2006,** *6* (4), 839-842.
7. Zheng, G.; Li, W.; Wang, X.; Wu, D.; Sun, D.; Lin, L., Precision Deposition of a Nanofibre by Near-Field electrospinning. *J. Phys. D: Appl. Phys.* **2010,** *43* (41), 415501-415506.
8. Chang, C.; Limkrailassiri, K.; Lin, L., Continuous Near-Field Electrospinning for Large Area Deposition of Orderly Nanofiber Patterns. *Appl. Phys. Lett.* **2008,** *93* (12), 123111-123113.
9. Visser, J.; Melchels, F. P.; Jeon, J. E.; Van Bussel, E. M.; Kimpton, L. S.; Byrne, H. M.; Dhert, W. J.; Dalton, P. D.; Hutmacher, D. W.; Malda, J., Reinforcement of Hydrogels Using Three-Dimensionally Printed Microfibres. *Nat. Commun.* **2015,** *6*.
10. Chen, F.; Hochleitner, G.; Woodfield, T.; Groll, J.; Dalton, P. D.; Amsden, B. G., Additive Manufacturing of a Photo-cross-linkable Polymer via Direct Melt Electrospinning Writing for Producing High Strength Structures. *Biomacromolecules* **2015,** *17* (1), 208-214.
11. Farrugia, B. L.; Brown, T. D.; Upton, Z.; Hutmacher, D. W.; Dalton, P. D.; Dargaville, T. R., Dermal Fibroblast Infiltration of Poly (ε-caprolactone) Scaffolds Fabricated by Melt Electrospinning in a Direct Writing Mode. *Biofabrication* **2013,** *5* (2), 025001-025011.
12. Hochleitner, G.; Jüngst, T.; Brown, T. D.; Hahn, K.; Moseke, C.; Jakob, F.; Dalton, P. D.; Groll, J., Additive Manufacturing of Scaffolds with Sub-micron Filaments via Melt Electrospinning Writing. *Biofabrication* **2015,** *7* (3), 035002-035011.